





## Design of next-generation therapeutic IgG4 with improved manufacturability and bioanalytical characteristics

Zhiqiang Chen<sup>a</sup>, Yueming Qian <sup>a</sup>, Yuanli Song <sup>a</sup>, Xuankuo Xu <sup>a</sup>, Li Tao<sup>b</sup>, Nesredin Mussa<sup>a</sup>, Sanchayita Ghose<sup>a</sup>, and Zheng Jian Li <sup>a</sup>

<sup>a</sup>Biologics Development, Global Product Development and Supply, Bristol Myers Squibb Company, Devens, MA, USA; <sup>b</sup>Biophysical Characterization, Global Product Development and Supply, Bristol Myers Squibb Company, New Brunswick, NJ, USA

### ABSTRACT

Manufacturability of immunoglobulin G4 (IgG4) antibodies from the Chemistry, Manufacture, and Controls (CMC) perspective has received little attention during early drug discovery. Despite the success of protein engineering in improving antibody biophysical properties, a clear gap still exists between rational design of IgG4 candidates and their manufacturing suitability. Here, we illustrate that undesirable two-peak elution profiles in cation-exchange chromatography are attributed to the S228P mutation (in IgG4 core-hinge region) intentionally designed to prevent Fab-arm exchange. A new scaffolding platform for engineering IgG4 antibodies amenable to bioprocessing and bioanalysis is proposed by introducing an “IgG1-like” single-point mutation in the hinge or CH1 region of IgG4S228P. This work offers insight into the design, discovery, and development of innovative therapeutic antibodies that are well suited for robust biomanufacturing and quality control.

### ARTICLE HISTORY

Received 7 July 2020  
Revised 23 August 2020  
Accepted 10 September 2020

### KEYWORDS

therapeutic IgG4; single-point mutation; manufacturability; bioprocessing; bioanalysis

### Introduction

Human IgG4 and Fc-null IgG1 are the preferred therapeutic antibody isotypes when Fc-mediated effector functions are undesirable.<sup>1</sup> However, *in vivo* studies have shown that human wild-type IgG4 can crosslink two different antigens<sup>2</sup> by swapping its half-molecule with another half-molecule from a different antibody, a process known as antigen-binding fragment (Fab)-arm exchange,<sup>3</sup> leading to random bispecific IgG4 molecules. The susceptibility to Fab-arm exchange can be a major disadvantage of wild-type IgG4 human immunotherapies, causing unpredictable specificity, pharmacokinetics, efficacy, and pharmacodynamics.<sup>4</sup>

Fab-arm exchange propensity of wild-type IgG4 monoclonal antibodies (mAbs) is due to their relatively flexible hinge region, which allows rapid intra-chain disulfide scrambling.<sup>5</sup> To avoid IgG4 Fab-arm exchange, the amino-acid sequence of IgG1 hinge region is referenced to substitute a proline for a serine in the hinge region of wild-type IgG4 mAbs, where the core-hinge motif CPSC is changed to CPPC (i.e., S228P) for improved structural rigidity.<sup>6,7,8</sup> This strategy has been applied to several marketed anti-programmed death-1 IgG4 therapeutics,<sup>8,9,10</sup> including nivolumab (OPDIVO<sup>®</sup>) and pembrolizumab (KEYTRUDA<sup>®</sup>), and a number of other IgG4 mAbs in preclinical or clinical studies.<sup>11</sup>

Despite its biological advantages, the S228P design has a major drawback in bioprocessing of IgG4 mAbs. Here, we report our investigation of a chromatographic phenomenon associated with the core-hinge design, and provide a molecular-level understanding to effectively mitigate the

issue by engineering new IgG4 scaffolds and performing molecular modeling.

### Results

#### Impact of core-hinge CPPC design

It has been observed that the CPPC motif of IgG4S228P mAbs poses challenges to biologics manufacturing during the cation-exchange chromatography (CEX) step,<sup>12,13,14,15</sup> where purified product can elute in two distinct peaks (i.e., two-peak elution, TPE) instead of one smooth peak as normally expected (**SI Appendix, Fig. S1**). Among the mAbs (six IgG1 and six IgG4) evaluated here, only IgG4S228P mAbs displayed the TPE behavior (**Figure 1b**), whereas all six IgG1 mAbs (**Figure 1a**) and the two wild-type IgG4 mAbs containing the CPSC motif (e.g., mAb7-w, and mAb12-w) (**Figure 1c**) showed the single-peak CEX elution behavior. It should be noted that the small shoulder peak to the lower right of the main peak (e.g., mAb4, mAb12, and mAb12-w) was due to minor charge variant species. For IgG4S228P mAbs, an isocratic elution condition corresponding to that for the early eluting peak (lower salt or conductivity) often leads to severe tailing and a large product pool volume (**SI Appendix Fig. S2**), affecting product manufacturability. However, an isocratic elution condition corresponding to that for the late eluting peak (higher salt or conductivity) often leads to inadequate impurity removal (**SI Appendix Table S1**), affecting product quality. In addition, results from our study revealed that the relative mass ratio of the two peaks is sensitive to even small changes in CEX operating conditions (e.g., pH) (**SI Appendix Fig. S3**). The dynamic TPE

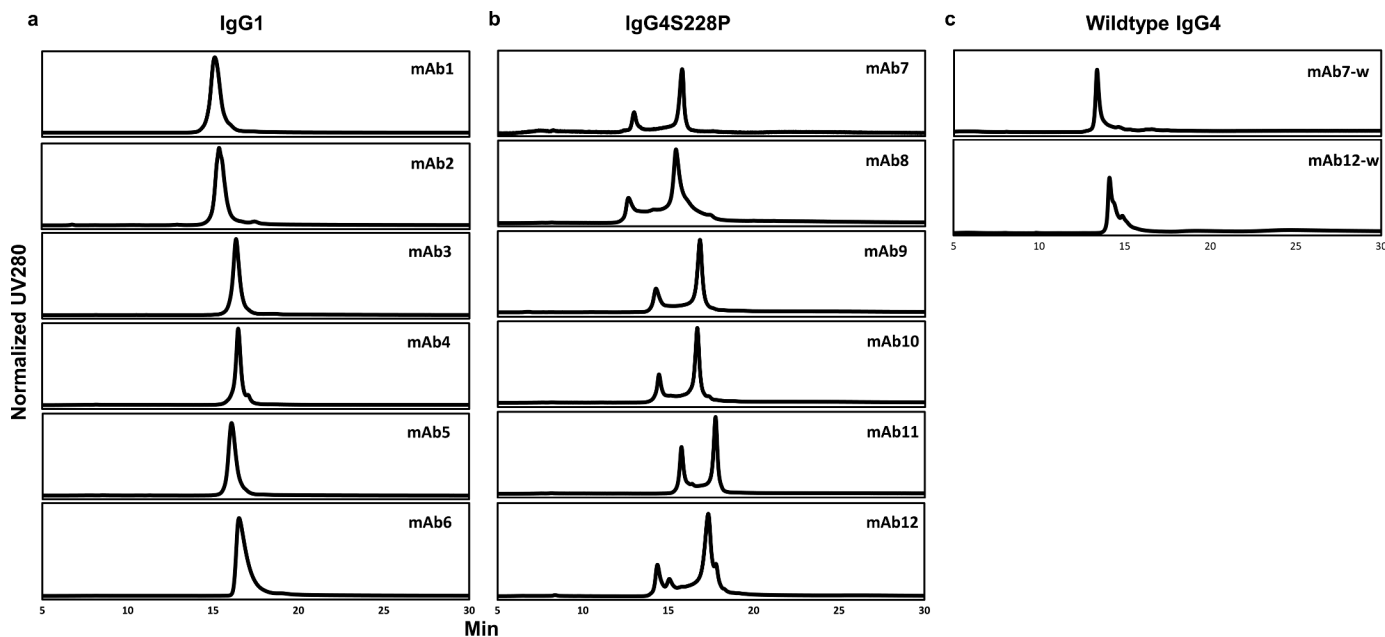


**Figure 1.** S228P mutation in hinge region of IgG4 mAbs led to the two-peak elution (TPE) behavior in CEX. (a) Single-peak elution was observed for IgG1 and (c) wild-type IgG4 mAbs. (b) The TPE behavior was observed for all the IgG4S228P mAbs studied. The small shoulder peak to the lower right of the main peak (e.g. mAb4, mAb12, and mAb12-w) was due to minor charge variant species. The CEX-HPLC column was packed with Propac SCX-10 resin (Thermo Fisher Scientific), with a column volume of 0.8 mL and an average particle size of 10  $\mu\text{m}$ . The salt gradient elution was from 20 mM MES, pH 5.0 to 20 mM MES, 1 M NaCl, pH 5.0 in 60 mins at a flow rate of 0.25 mL/min with a constant injected protein mass of 10  $\mu\text{g}$ .

phenomenon may indicate the presence of mutually convertible product populations of different conformations, adding another degree of complexity to process control during commercial manufacturing. The TPE behavior of IgG4S228P mAbs also causes difficulties in characterizing product charge variants when ion-exchange-based analytical methods are used for quality control. This issue manifests itself even more for combination therapies (*SI Appendix Fig. S4*), which have shown to be a promising new therapeutic platform presented to patients as the combination of two or more mAbs in a single vial.<sup>16,17,18</sup>

Using mAb11, an IgG4S228P mAb, the two CEX elution peaks (*Figure 1b*) were fractionated and characterized. These two fractions were found to have the same molecular size and purity by size exclusion chromatography (SEC) (*SI Appendix Fig. S5*), as well as very comparable charge variant profiles by imaged capillary isoelectric focusing (iCIEF) analysis (*SI Appendix Fig. S6*). In a similar study using mAb9, also an IgG4S228P mAb, intact mass analysis (data not shown) revealed no differences in product mass identity between its two CEX elution peaks. Moreover, once re-loaded onto the CEX column, each of the two peaks continued to show the same TPE pattern as that for the original load material (*SI Appendix Fig. S7*). These results suggested the co-existence of structurally distinct but thermodynamically interchangeable mAb conformations that differ in CEX retention properties.

### Identification of critical mAb region

Enzyme digestion (see **Materials and methods** section) using pepsin- and papain-immobilized agarose resins was performed to generate mAb11 F(ab')<sub>2</sub> and Fab fragments, respectively, in order to evaluate the contribution of different mAb regions to

the observed TPE behavior. High-purity F(ab')<sub>2</sub> and Fab fragments, as confirmed by SEC-HPLC (*SI Appendix Fig. S8*), were separately loaded onto the CEX column, where only the F(ab')<sub>2</sub> displayed the TPE behavior (*Figure 2a*). The similar peak retention times between mAb11 and mAb11 F(ab')<sub>2</sub> indicated that the Fc region is not much involved in the binding events that determine the overall mAb-resin interactions. Scapin et al.<sup>8</sup> hypothesized that the shorter and more compact hinge region of IgG4S228P (compared with the IgG1 hinge), as well as the steric constraints to which the hinge is subjected, causes an approximately 120° rotation of the CH2 domain and solvent-exposure of the glycan structures. Our results are consistent with the notion that the CH2 domain wrapped with hydrophilic and neutral glycans substantially reduces the involvement of the Fc region in charge-mediated mAb adsorption to CEX resins. The single-peak elution profile (*Figure 2a*) of the mAb11 Fab (with no hinge) and the TPE profile of the F(ab')<sub>2</sub> (*Figure 2a*) suggested that the Fab alone does not contribute to the TPE behavior. The single-peak elution profile of a fusion protein comprising an IgG4-Fc region and the CPPC core-hinge motif (*Figure 2a*) suggested that the Fc region coupled with CPPC-core hinge is not contributing to the TPE behavior either. The above observations collectively indicated that the TPE behavior is directly associated with F(ab')<sub>2</sub> where both the Fab and CPPC-core hinge play critical roles.

### Conformational energy modeling

Molecular modeling was used to provide possible mechanistic explanation for the TPE phenomenon by comparing the conformational energies for IgG4S228P and the two IgG types (i.e., IgG1 and wild-type IgG4) that did not have the TPE behavior.

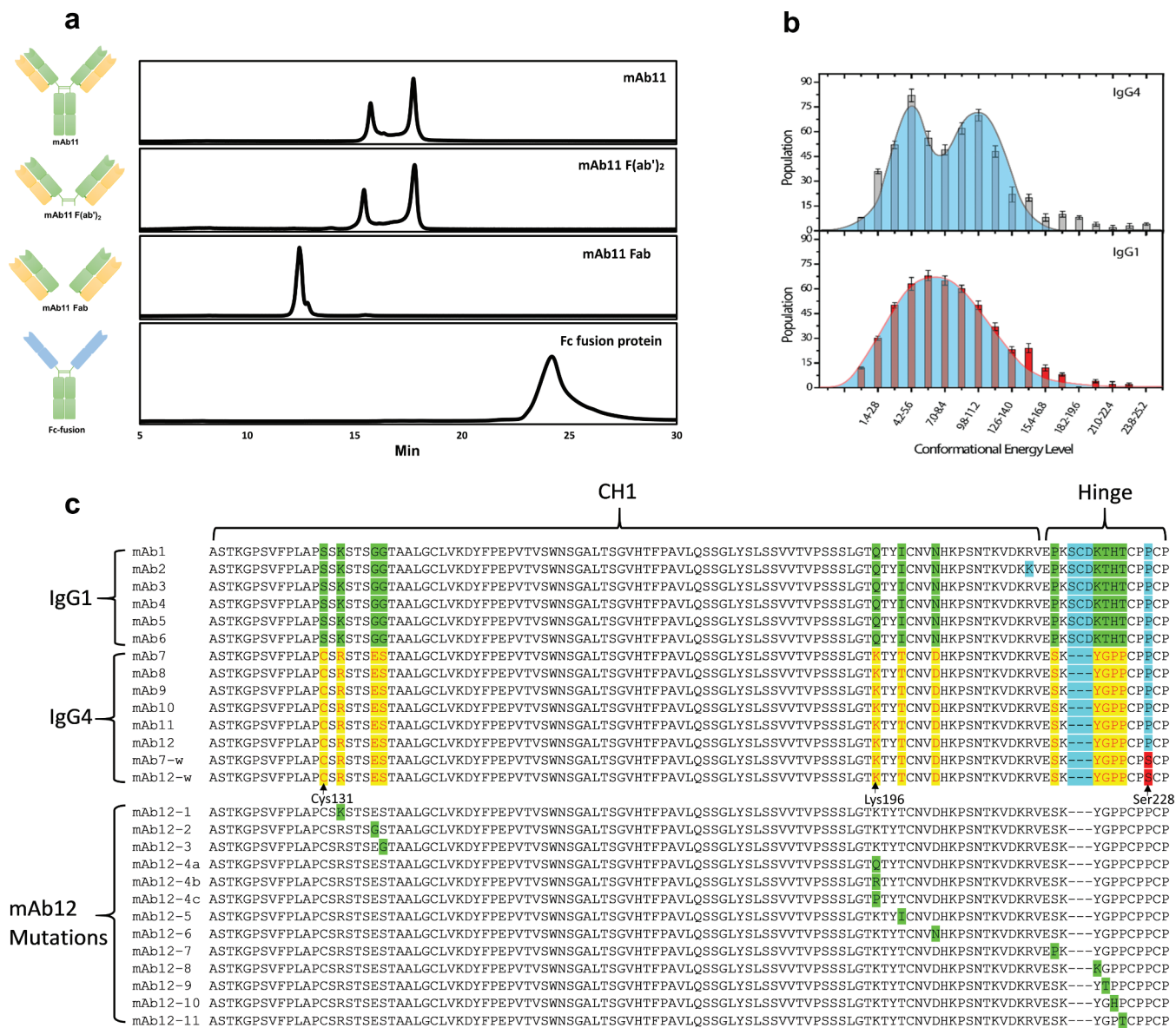


**Figure 2.** Design of next-generation therapeutic IgG4 mAbs using protein engineering. (a) CEX-HPLC chromatogram for mAb11, mAb 11 fragments and a fusion protein containing a fully human IgG4-Fc region and the CPPC core-hinge motif. The two-peak elution (TPE) behavior was observed for mAb11 and mAb11 F(ab)<sub>2</sub>, but not for mAb 11 Fab and the Fc-fusion protein, suggesting that the TPE behavior may be primarily attributed to F(ab)<sub>2</sub>. (b) Conformational energies for IgG1 (mAb1) and IgG4S228P (mAb12). Two distinct conformational energy levels were observed for IgG4S228P (mAb12), while only one was observed for IgG1 (mAb1). (c) Sequence alignment of the constant heavy chain 1 (CH1) and hinge region for IgG1, IgG4S228P, and two wild-type IgG4 (mAb7-w and mAb12-w) with the CPPC motif in the core-hinge region. Twelve amino acid differences were found between IgG1 and IgG4S228P mAbs. C131 in IgG4 forms the inter-chain disulfide bond between heavy and light chains, thus cysteine was not mutated to the corresponding serine to preserve intact IgG4 structure. The other eleven amino acids in IgG4S228P were mutated individually to the corresponding amino acids in IgG1 to evaluate their CEX behavior. Additionally, K196 was further mutated to K196R and K196P to generate mAb12-4b and mAb12-4c in addition to mAb12-4a.

Conformational ensemble (see **Materials and Methods** section)<sup>19</sup> results suggested that there are two dominant populations of the conformational energy distribution for IgG4S228P, but only one major population for IgG1 and wild-type IgG4 (Figure 2b and SI Appendix Fig. S9a). In addition, the two energy populations of IgG4S228P largely correspond to two major conformational categories, termed qualitatively as T-shaped and Y-shaped antibody structures (data not shown).<sup>20</sup> It is hypothesized that the relatively rigid core-hinge region of IgG4S228P hinders the dynamic interchange among the mAb structures different in conformational energy levels owing to high activation energy barrier. Instead, the

more flexible hinge region of IgG1 and wild-type IgG4 allows the conversion among conformational intermediates to occur more readily. Overall, we infer that, due to the lack of hinge region flexibility, the two distinctive energy states of IgG4S228P molecules affect the inherent CEX retention characteristics of this mAb subtype and ultimately lead to the observed TPE behavior.

### Strategies for solving the TPE issue

In an effort to improve the manufacturability of IgG4S228P mAbs, we performed single-point mutagenesis to generate

variants of mAb12 (an IgG4S228P mAb) using IgG1 as the amino-acid sequence template. Mutations were designed based only on the sequence alignment of the hinge and CH1 regions between all the IgG4S228P and IgG1 mAbs studied in this work. Other mAb regions, such as the Fc, kappa light chain, and variable heavy chain ( $V_H$ ), were not considered for single-point mutagenesis because: 1) results in **Figure 2a** indicated the Fc region is not much involved in the IgG4-CEX interactions; 2) all the IgG4S228P and IgG1 mAbs in **Figure 1** share the same constant kappa light chain despite their different CEX elution behaviors; and 3) each mAb regardless of subtype has a unique  $V_H$ , therefore, this region is unlikely to cause the subtype-dependent TPE behavior.

### Engineering IgG4 scaffolds

In the hinge and CH1 regions, 12 amino-acid differences were found between the IgG4S228P and IgG1 mAbs, as shown in **Figure 2c**. IgG4S228P C131 forms the inter-chain disulfide bond between heavy and light chains, and thus it was not mutated in order to preserve the intact IgG4 structure. The other identified differences were studied individually by single-point replacement of the amino acids in IgG4 with the corresponding ones in IgG1, and the resulting mAb12 mutants were examined for their CEX elution behavior. In addition, K196 was mutated to K196R and K196P to further explore the impact of amino-acid side chain characteristics on the molecular property of interest. DNA sequencing (data not shown) and mass spectrometry (MS) analysis (**SI Appendix Fig. S10**) confirmed the correct identity of the mutants. Five of the 13 mutants, one with mutation in the CH1 domain (mAb12-4c) and four in the hinge region (mAb12-7, mAb12-9, mAb12-10, and mAb12-11), surprisingly showed the single-peak CEX elution behavior (**Figure 3a**), while the others still displayed the TPE pattern (**SI Appendix Fig. S11**).

Subsequently, *in vitro* studies were performed to evaluate the Fab-arm exchange propensity for these five mutants exhibiting the single-peak CEX elution behavior. Using mAb12-w and mAb12 as positive and negative controls, respectively, mAb12-4c, mAb12-7, mAb12-9, mAb12-10, and mAb12-11 were each mixed with mAb7-w in equal amounts, and tested with liquid chromatography (LC)-MS for bispecific antibody formation after a 24-hr incubation at 37°C with and without 0.5 mM reduced glutathione (GSH). As reported previously,<sup>3</sup> *in vitro* Fab-arm exchange between two wild-type IgG4 mAbs requires the presence of 0.5 mM GSH. The mixture of mAb12-w (148404 Da) and mAb7-w (major N-glycan species: G0F/G0F of 147166 Da, G0F/G1F of 147328 Da, and G1F/G1F of 147489 Da) showed no additional mass species without GSH (**Figure 3b**); however, intermediate masses (147784 Da and 147986 Da) were found in the presence of GSH (**Figure 3c**), providing clear evidence of Fab-arm exchange.<sup>21</sup> These two intermediate species had the expected masses of mAb12-w/mAb7-w G0F and mAb12-w/mAb7-w G1F bispecific antibodies, respectively. LC-MS data of the mAb12/mAb7-w mixture (**Figure 3d**) confirmed that the S228P mutation of mAb12 indeed prevented *in vitro* Fab-arm exchange owing to the rigid CPPC core-hinge motif. In comparison, mutants mAb12-4c, mAb12-7, mAb12-9, mAb12-10, and mAb12-11 not only effectively prevented Fab-arm exchange (**Figure 3e-i**), but also exhibited the single-peak CEX elution profile representing improved manufacturability. Unlike IgG4S228P, these five mAb12 mutants showed one major energy population (**SI Appendix Fig. S9b and S9c**) as seen for IgG1s (**Figure 2**) and wild-type IgG4s (**SI Appendix Fig. S9a**) by the molecular modeling. Mutants mAb12-4 c, mAb12-9, mAb12-10, and mAb12-11 maintained comparable antigen-binding activity (enzyme-linked immunosorbent assay (ELISA) binding measurements) to that of the control (mAb12), while mutant mAb12-7 showed a slightly lower potency (46%) (**Figure 3j**,

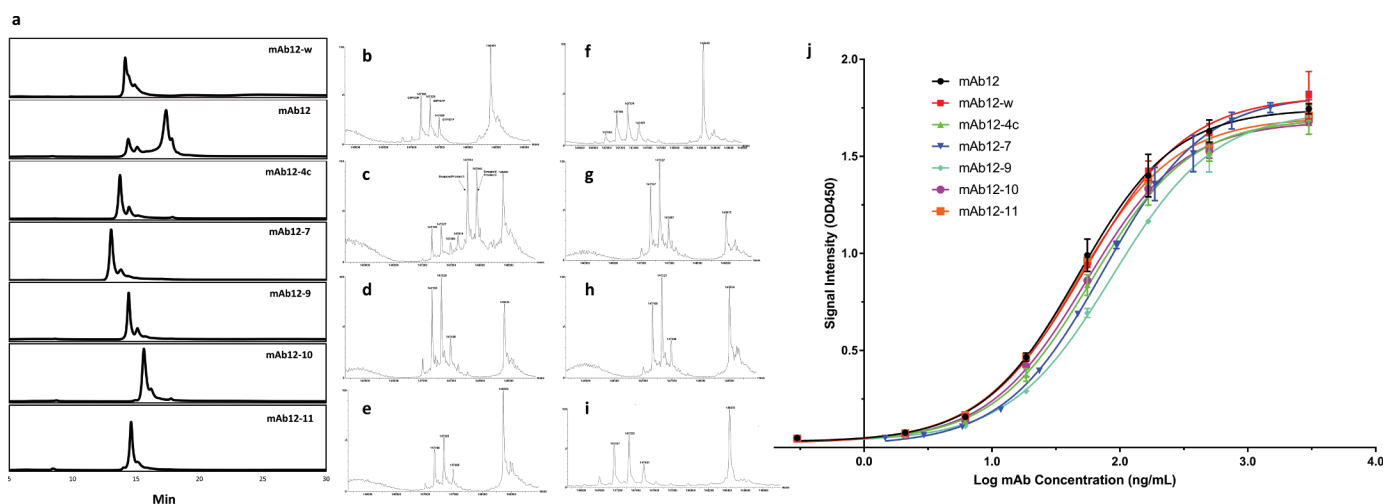


**Figure 3.** Successful design of IgG4 mutations with improved manufacturability and bioanalytical characteristics. (a) Single-peak CEX elution behavior was observed for mAb12-4c, mAb12-7, mAb12-9, mAb12-10, and wild-type mAb12-w (mAb12 without the S228P mutation in the core-hinge region). The TPE behavior was observed for mAb12. (b) The mixture of mAb12-w/mAb7-w was incubated for 24 hrs in the absence of 0.5 mM GSH at 37°C, and subsequently analyzed by LC-MS. The wild type mAb7-w contained various glycosylation species (G0F/G0F, G0F/G1F and G1F/G1F). The mixtures of mAb12-w/mAb7-w (c), mAb12/mAb7-w (d), mAb12-4c/mAb7-w (e), mAb12-7/mAb7-w (f), mAb12-9/mAb7-w (g), mAb12-10/mAb7-w (h), and mAb12-11/mAb7-w (i) were incubated for 24 hrs in the presence of 0.5 mM GSH at 37°C, and subsequently analyzed by LC-MS. (j) ELISA binding potency of the mutants. Absorbance at 450 nm was plotted against log ng/mL of mutant concentration, with error bars obtained from duplicate measurements. The relative potency for each mutant was calculated and shown in **SI Appendix Table S2**.

**Table S2).** Considering that these single-point mutations only occurred in the hinge or CH1 region, the Fc mediated effector functions are not expected to be significantly altered.<sup>20,22</sup> This was confirmed by the IgG4-FcγRI interaction studies using biolayer interferometry (BLI). The BLI data (*SI Appendix Fig. S12*) suggested that the binding affinity of these five mAb12 mutants to FcγRI is very similar to that of mAb12-w.

## Discussion

While the current generation of IgG4S228P mAbs effectively avoids Fab-arm exchange, the IgG4S228P design leads to the undesired TPE behavior in CEX, creating substantial challenges to biologics manufacturing and analytical development. The next-generation IgG4 design reported here can mitigate these issues by incorporating single-point mutations in the hinge or CH1 (K196P) region. As single-point mutations in IgG4S228P may change molecular properties, the developability of IgG4 candidates should be carefully assessed for CMC during molecular design and discovery of IgG4 candidates. Targeted mutations against other subclasses may be an effective strategy to improve molecular properties by acquiring unique features of other IgG subclasses.

## Materials and methods

### CEX-HPLC method

Analytical CEX-HPLC was performed using a ProPac SCX-10 LC column from Thermo Fisher Scientific (Wilmington, DE, USA) installed on a Waters HPLC system from Waters Corporation (Milford, MA, USA). The method used was a salt gradient elution from 20 mM MES, pH 5.0 to 20 mM MES, 1 M NaCl, pH 5.0 in 60 min at a flow rate of 0.25 mL/min with a constant injected protein mass of 10 µg. The eluted protein was monitored by UV 280 nm.

### SEC method for purity and size analysis

Analytical SEC was performed using a TSKgel G3000SWXL column (14 mL and an average particle size of 5 µm) from Tosoh Bioscience (King of Prussia, PA, USA) installed on a Waters HPLC system from Waters Corporation (Milford, MA, USA). The method used a mobile phase containing 100 mM sodium phosphate, 100 mM sodium sulfate, pH 6.8, at a flow rate of 1 mL/min, with a constant injected protein mass of 100 µg. The eluted protein was monitored by UV 280 nm.

### Chromatography instrumentation and methods

All chromatography runs were performed on a GE Healthcare ÄKTA avant system installed with Unicorn software version 6.3 (Piscataway, NY, USA). POROS XS resin was packed in Omnifit® columns (0.66 cm I.D × 10 cm bed height) purchased from Fisher Scientific (Hampton, NH, USA). The packed and conditioned column was equilibrated with 5 column volumes (CV) of 25 mM MES buffer, pH 5.0. The CEX column was loaded to a loading of 1 mg/mL resin at pH 5, followed by a 30 CV 0–1 M NaCl gradient in 20 mM MES buffer at pH 5. The

column was regenerated with 3 CV of 1 M NaCl, sanitized with 3 CV of 1 M NaOH, and stored in 0.1 M NaOH. Protein concentration was measured using a NanoDrop 2000 purchased from Thermo Fisher Scientific (Wilmington, DE, USA). All runs were performed at room temperature.

### iCIEF method

iCIEF was performed using an iCE280 Analyzer (Convergent Bioscience, Toronto, Canada) to quantify product charge variants. The separation cartridge along with capillary was purchased from Convergent Bioscience. This capillary was fixed onto a glass substrate and separated from the catholyte and anolyte by two pieces of hollow fiber membrane. An IgG sample was prepared by mixing 2 mg/mL IgG with various pI markers, 1% methyl cellulose solution, and pharmalyte 3–10, before diluted with deionized water. The mixture was centrifuged and supernatant was focused in station for varied lengths of time to achieve the optimum resolution. The final image of the IEF trace was captured by the 280 nm deuterium lamp detector.

### Preparation of F(ab')<sub>2</sub> domain of mAb11 using pepsin digestion

Agarose-immobilized pepsin was purchased from Thermo Fisher Scientific (Waltham, MA, USA). The mAb11 sample was digested by pepsin-agarose (0.25 mL pepsin-agarose per 20 mg mAb11) at pH 4.5 in a 37°C water bath for 4 h. The digested product was adjusted to pH 7.0 and then purified by flowing through a Protein A column (packed with MabSelect Sure resin) pre-equilibrated at pH 7.0. The small Fc fragments were washed away during 10 mM Tris•HCl, pH 7 buffer wash, and the F(ab')<sub>2</sub> was collected during 25 mM sodium phosphate, 150 mM sodium chloride, pH 7.2 buffer wash. The undigested mAb and Fc fragments were retained on the column and stripped with an acetic acid solution. Then, the column was sanitized with a solution containing 20 mM sodium hydroxide and 1.0% benzyl alcohol buffer.

### Preparation of Fab domain of mAb11 using papain digestion

Agarose-immobilized papain was purchased from Thermo Fisher Scientific (Waltham, MA, USA). The mAb11 sample was digested by papain-agarose (0.25 mL papain agarose per 10 mg mAb11) in 20 mM sodium phosphate, 20 mM cysteine•HCl, 10 mM EDTA at pH 7 in a 37°C water bath for 4 h. The Fab was separated from undigested mAb and Fc fragments using a Protein A column packed with MabSelect SuRe resin (GE Healthcare).

### Cell line and culture conditions

ExpiCHO-S cells (Thermo Fisher Scientific) were grown in defined and serum-free ExpiCHO expression medium (Thermo Fisher Scientific) and passaged in shake flasks every 3 d. Cells were incubated at 130 rpm on an orbital shaker platform in a 37°C incubator with a humidified atmosphere of 8% CO<sub>2</sub>.

## Mutant construction and transient expression of mAbs in Chinese hamster ovary cells and purification

Site-directed mutagenesis and antibody transient expression were performed as previously described.<sup>23</sup> In brief, the template DNA of mAb12 plasmid was methylated prior to the mutagenesis reaction, in which two overlapping primers were used and one of them contained the target mutation. The mutagenesis products were transformed into *E. coli* competent cells, where unmethylated linear mutated DNA was circularized and replicated. Plasmid DNAs were isolated and purified with a PureLink Hi Pure Plasmid Maxiprep kit (Thermo Fisher Scientific). For each antibody or mutant, 50 µg of plasmid DNA were used to transfect 50 mL of ExpiCHO-S culture in a 250 mL shake flask using ExpiFectamine CHO Reagent (Thermo Fisher Scientific). The transfected culture was fed with ExpiCHO Feed (Thermo Fisher Scientific) and ExpiCHO Enhancer (Thermo Fisher Scientific), accordingly. Both mAb12 and its mutants were robustly expressed in ExpiCHO-S transient expression system, indicating that amino-acid replacements in the target regions did not affect IgG4 synthesis. All mAbs expressed in Chinese hamster ovary cells were purified using a Bristol Myers Squibb platform Protein A affinity chromatography method from cell harvest. Purified mAbs were subject to further studies.

## ELISA binding assay

The assay plates were coated with 100 µL (2 µg/mL) of human mAb12 murine IgG2 (prepared in-house) in bicarbonate buffer for 1 hr at room temperature. The plates were then blocked with 300 µL of SeaBlock solution (Pierce # 37527) for 1 hr at room temperature. Reference material and the samples were diluted to 1 µg/mL in Teknova assay diluent buffer (Teknova- # D5120) followed by two-fold serial dilutions.

The blocking buffer was decanted and plate washed three times with 300 µL of wash buffer phosphate-buffered saline-0.1% Tween (PBS-T). The samples and reference standards (100 µL) were added to the plate and incubated for 1 hr at room temperature. After three washes the 100 µL of Secondary Antibody (anti-human IgG4 Fc, HRP; 1:1000 in Teknova diluent), purchased from Thermo Fisher (Cat# MH1742), was added and incubated for 1 hr at room temperature.

After washing, 100 µL of Dako TMB was added and incubated for 10 min. The reaction was stopped with 100 µL of 1 N sulfuric acid. The absorbance was read at 450 nm with 650 nm as background correction using Softmax software on M5 plate reader (Molecular Devices). The EC<sub>50</sub> values were calculated from the absorbance values vs. log concentrations of samples and reference at each dilution. The percent relative binding potency was calculated by dividing the reference material EC<sub>50</sub> by the test sample EC<sub>50</sub> as a percentage.

## Non-reduced intact mass analysis

The LC-MS was performed with an Acquity UHPLC coupled with a quadrupole time-of-flight (Q-ToF) mass spectrometer (Waters, Milford, MA). The capillary voltage for the Q-ToF was set at 3000 V and the sample cone voltage at 80 V. The method for analysis was the same as described previously.<sup>24</sup> The sample was

injected at 0.5 µg onto a reversed phase column (10 µm, 2.1 × 100 mm POROS®, Applied Biosystems, Foster City, CA) equilibrated with 20% acetonitrile containing 0.1% formic acid, followed by a gradient elution from 20% to 50% acetonitrile in 25 min, at a flow rate of 0.25 mL/min. The mass spectra were scanned from m/z 500 to 4000; the combined data were then deconvoluted using MaxEnt1 algorithm (Waters, Milford, MA).

Fab-arm exchange condition: mAb12 mutation was mixed with mAb7-w and incubated with 0.5 mM GSH (Sigma) in degassed PBS (pH 7.2). The final concentration of both mAb12 mutation and mAb7-w was 20 µg/mL. The mixtures (70 µL) were incubated at 37°C for 24 h. The samples were then stored at 4°C before intact mass testing.

## FcγR binding measurements

BLI experiments were performed on an Octet QK96 (ForteBio, Fremont, CA) instrument at room temperature. After a 60-s equilibrium step of a Protein A-coated sensor (Part Cat 18-5010), mAb12-w, its mutants, and mAb1 with a fixed concentration of 20 µg/mL were immobilized for 60 seconds on the protein A-coated surface. Nonspecific interacting mAb was washed away to the same baseline during a 60-s wash step. The immobilized mAbs were associated to FcγRI recombinant protein with a series of 7 concentrations from 6 to 185 µM for 100 seconds, followed by a 150-s dissociation step. The binding between FcγRI and the mAb samples were plotted and analyzed using an Octet data analysis software version 7.0 (ForteBio, Fremont, CA). Reference was used with FcγRI loaded Protein A-coated surface incubated in the assay buffer instead of the analyte (mAb samples).

## Ensemble generation and analysis for mAbs

Ensembles of conformation of IgG1, IgG4, and IgG4 mutants were generated with RANCH program, which is a program that generates a pool of independent models based upon sequence and structural information.<sup>25</sup> Symmetry was set as P1 in all runs. Previous structural studies suggested the hinge region flexibility of IgG1 is higher than that of IgG4.<sup>8,20</sup> The length of IgG hinge region and its proline composition also suggest that this region is more flexible in IgG1. IgG1 and IgG4 were set as three domains including two Fab domains and one Fc domain. The three domains, allowed to move in conformation pool generation, were linked to the core-hinge region with the CPPCP motif in IgG1 and the PPCPPCP motif in IgG4. Hinge regions were fixed in conformation generation. Each conformation generation run generated 10000 conformations. The conformational energy of each conformation was calculated using all atom force field OPLS-AA.<sup>19</sup> Conformational energy was statistically analyzed using an energy level of 1.4 kcal/mol, which is the hydrogen bond energy level at room temperature.<sup>26</sup> The number of conformations in each energy level was plotted as a function of conformational energy levels.

## Acknowledgments

The authors are grateful to Dr. Jinmei Fu. Her specialty in intact mass spectrometry greatly helped this project. Sadly, Dr. Fu passed away before the completion of this manuscript. This manuscript is dedicated to her. The

author would like to thank Dr. Xin Huang, Dr. Xuning Wang, Dr. Stefan Kirov and Dr. Kandasamy Ravi for their support on DNA sequence confirmation of the mutants, Dr. Satish Sharma for support on ELISA binding assay, Dr. Mengxiao Lu for support on iCIEF. The authors would also like to thank Dr. Jeff Beckman, Dr. Zhijun Tan, Dr. Chao Huang, Dr. Shrikant Deshpande and Dr. Karla Henning for helpful discussion and valuable comments.

## Disclosure of potential conflicts of interest

No potential conflicts of interest were disclosed.

## ORCID

Yueming Qian  <http://orcid.org/0000-0001-7340-6421>

Yuanli Song  <http://orcid.org/0000-0002-5078-8049>

Xuankuo Xu  <http://orcid.org/0000-0002-5557-0284>

Zheng Jian Li  <http://orcid.org/0000-0002-1941-4145>

## Author contributions

Z.C. and X.X. designed the study; Z.C. performed the experiments; X. X. supervised the research. Y.Q. generated all the mutants; Y.S. performed the molecular simulation and FcγRI measurements; Z.C., Y.Q., Y.S., X.X., T.L., N.M., S.G., Z.L. analyzed and interpreted the data; Z.C. and X. X. wrote the manuscript with comments from all authors. All authors reviewed and approved the final manuscript.

## Competing interests

Patent applications based on this work have been filed by Bristol Myers Squibb Company.

## Abbreviations

BLI	Bilayer interferometry
CEX	Cation-exchange chromatography
CHO	Chinese hamster ovary
CMC	Chemistry, Manufacture, and Controls
ELISA	Enzyme-linked immunosorbent assay
Fab	Antigen-binding fragment
Fc	Fragment crystallizable region
GSH	Glutathione
HPLC	High performance liquid chromatography
HRP	Horseradish peroxidase
iCIEF	Imaged capillary isoelectric focusing
IgG1	Immunoglobulin G1
IgG4	Immunoglobulin G4
LC	Liquid chromatography
mAb	Monoclonal antibody
MS	Mass spectrometry
SEC	Size exclusion chromatography
TPE	Two-peak elution
V <sub>H</sub>	Variable heavy chain

## References

- Offringa R, Glennie MJ. Development of next-generation immunomodulatory antibodies for cancer therapy through optimization of the IgG framework. *Cancer Cell*. 2015;28:273–75. doi:10.1016/j.ccell.2015.08.008.
- Schuurman J, Van Ree R, Perdok GJ, Van Doorn HR, Tan KY, Aalberse RC. Normal human immunoglobulin G4 is bispecific: it has two different antigen-combining sites. *Immunology*. 1999;97:693–98. doi:10.1046/j.1365-2567.1999.00845.x.
- van der Neut Kolfshoten M, Schuurman J, Losen M, Bleeker WK, Martinez-Martinez P, Vermeulen E, den Bleker TH, Wiegman L, Vink T, Aarden LA, et al. Anti-inflammatory activity of human IgG4 antibodies by dynamic Fab arm exchange. *Science*. 2007;317:1554–57. doi:10.1126/science.1144603.
- Silva JP, Vetterlein O, Jose J, Peters S, Kirby H. The S228P mutation prevents in vivo and in vitro IgG4 Fab-arm exchange as demonstrated using a combination of novel quantitative immunoassays and physiological matrix preparation. *J Biol Chem*. 2015;290(9):5462–69. doi:10.1074/jbc.M114.600973.
- Bloom JW, Madanat MS, Marriott D, Wong T, Chan SY. Intrachain disulfide bond in the core hinge region of human IgG4. *Protein Sci*. 1997;6:407–15. doi:10.1002/pro.5560060217.
- Angal S, King DJ, Bodmer MW, Turner A, Lawson ADG, Roberts G, Pedley B, Adair JR. A single amino acid substitution abolishes the heterogeneity of chimeric mouse/human (IgG4) antibody. *Mol Immunol*. 1993;30:105–08. doi:10.1016/0161-5890(93)90432-B.
- Beck A, Wurch T, Bailly C, Corvaia N. Strategies and challenges for the next generation of therapeutic antibodies. *Nat Rev Immunol*. 2010;10:345–52. doi:10.1038/nri2747.
- Scapin G, Yang X, Prorise WW, McCoy M, Reichert P, Johnston JM, Kashi RS, Strickland C. Structure of full-length human anti-PD1 therapeutic IgG4 antibody pembrolizumab. *Nat Struct Mol Biol*. 2015;22:953–58. doi:10.1038/nsmb.3129.
- Wang C, Thudium KB, Han M, Wang XT, Huang H, Feingersh D, Garcia C, Wu Y, Kuhne M, Srinivasan M, et al. In vitro characterization of the anti-PD-1 antibody nivolumab, BMS-936558, and in vivo toxicology in non-human primates. *Cancer Immunol Res*. 2014;2:846–56. doi:10.1158/2326-6066.CIR-14-0040.
- Davies AM, Sutton BJ. Human IgG4: a structural perspective. *Immunol Rev*. 2015;268:139–59. doi:10.1111/imr.12349.
- Reichert JM. Antibodies to watch in 2017. *mAbs*. 2017;9:167–81. doi:10.1080/19420862.2016.1269580.
- Luo H, Cao M, Newell K, Afdahl C, Wang J, Wang WK, Li Y. Double-peak elution profile of a monoclonal antibody in cation exchange chromatography is caused by histidine-protonation-based charge variants. *J Chromatogr A*. 2015;1424:92–101. doi:10.1016/j.chroma.2015.11.008.
- Guo J, Creasy AD, Barker G, Carta G. Surface induced three-peak elution behavior of a monoclonal antibody during cation exchange chromatography. *J Chromatogr A*. 2016;1474:85–94. doi:10.1016/j.chroma.2016.10.061.
- Farys M, Gibson D, Lewis AP, Lewis W, Kucia-Tran R. Isotype dependent on-column non-reversible aggregation of monoclonal antibodies. *Biotechnol Bioeng*. 2018;115:1279–87. doi:10.1002/bit.26547.
- Dumet C, Pottier J, Gouilleux-Gruart V, Watier H. Insights into the IgG heavy chain engineering patent landscape as applied to IgG4 antibody development. *mAbs*. 2019;11:1341–50.
- Mahoney KM, Rennert PD, Freeman GJ. Combination cancer immunotherapy and new immunomodulatory targets. *Nat Rev Drug Discov*. 2015;14:561–84.
- Larkin J, Hodi FS, Wolchok JD. Combined nivolumab and ipilimumab or monotherapy in untreated melanoma. *N Engl J Med*. 2015;373:1270–71. doi:10.1056/NEJMoa1504030.
- Alan J, NL K, Fontana DJ, Gutierrez AA, Selby MJ, Lewis KE. U.S. Application. No. US20160222116A1. 2016.
- Robertson MJ, Tirado-Rives J, Jorgensen WL. Improved peptide and protein torsional energetics with the OPLS-AA force field. *J Chem Theory Comput*. 2015;11:3499–509. doi:10.1021/acs.jctc.5b00356.
- Tian X, Vestergaard B, Thorolfsson M, Yang Z, Rasmussen HB, Langkilde AE. In-depth analysis of subclass-specific conformational preferences of IgG antibodies. *IUCrJ*. 2015;2:9–18. doi:10.1107/S205225251402209X.
- Labrijn AF, Buijsse AO, van den Bremer ET, Verwilligen AY, Bleeker WK, Thorpe SJ, Killestein J, Polman CH, Aalberse RC, Schuurman J, et al. Therapeutic IgG4 antibodies engage in Fab-arm exchange with endogenous human IgG4 in vivo. *Nat Biotechnol*. 2009;27:767–71. doi:10.1038/nbt.1553.

22. Lu J, Chu J, Zou Z, Hamacher NB, Rixon MW, Sun PD. Structure of FcγRI in complex with Fc reveals the importance of glycan recognition for high-affinity IgG binding. *Proc Natl Acad Sci.* 2015;112:833–38. doi:10.1073/pnas.1418812112.
23. Qian Y, Chen Z, Huang X, Wang X, Xu X, Kirov S, Ludwig R, Qian N-X, Ravi K, Tao L, et al. Early identification of unusually clustered mutations and root causes in therapeutic antibody development. *Biotechnol Bioeng.* 2018;115:2377–82. doi:10.1002/bit.26728.
24. Fu J, Bongers J, Tao L, Huang D, Ludwig R, Huang Y, Qian Y, Basch J, Goldstein J, Krishnan R, et al. Characterization and identification of alanine to serine sequence variants in an IgG4 monoclonal antibody produced in mammalian cell lines. *J Chromatogr B Analyt Technol Biomed Life Sci.* 2012;908:1–8. doi:10.1016/j.jchromb.2012.09.023.
25. Bernado P, Mylonas E, Petoukhov MV, Blackledge M, Svergun DI. Structural characterization of flexible proteins using small-angle X-ray scattering. *J Am Chem Soc.* 2007;129(17):5656–64. doi:10.1021/ja069124n.
26. Smith JD, Cappa CD, Wilson KR, Messer BM, Cohen RC, Saykally RJ. Energetics of hydrogen bond network rearrangements in liquid water. *Science.* 2004;306:851–53. doi:10.1126/science.1102560.